Mechanical Behaviour Optimization of Titanium-Alloy-Reinforced PLA Using Taguchi-Driven FDM Parameter Selection

Senniangiri *Natarajan*[*], Kavyapriya *Saravanan*, Gangeshwaran *Gunasekeran*, and Raagul *Shanmugasundaram*

Department of Mechanical Engineering, Nandha Engineering College, Perundurai 638052, Tamil Nadu, India

Abstract. changes on the fractured surfaces. The results show that it is possible to 3D print using the eco-friendly 25%TAP-PLA, which is a major step toward the sustainability The primary aim of research is to find optimal fused deposition 3D printing settings by taguchi approach such that polylactic acid (PLA) reinforced with 25% titanium alloy powder. The optimization of process parameters and the L16 OA matrix based on Taguchi were both designed and executed using the Minitab program. Nozzle temperature (200ºC to 245ºC), layer thickness (120 µm to 420 µm), infill density (40–100%), concentric (C)), triangular (T), grid (G), infill patterns, (line (L) and Filament type (25% TAP-PLA) were all part of the experimental design. The test components were made using FDM and their tensile, flexural, and impact properties were evaluated according to ASTM standards (D-638, D-790, and D-256). According to the findings, the mechanical strength was primarily affected by the infill density. The optimal configuration for optimal results included a nozzle temperature of 230ºC, a layer thickness of 320 µm, an infill density of 100%, and a grid infill pattern. Together, these parameters provide tensile strength (TS) of 51.79 MPa, an impact strength (IS) of 16.98 kJ/m^2, and flexural strength (FS) of 91.69 MPa. In addition, scanning electron microscopy (SEM) was used to analyze morphological goals for 3D printing material utilization.

1 Introduction

3D printing is a new way to make prototypes quickly and easily. It uses concepts of computer-aided 3D modeling to create many different kinds of items. PLA–Al composites were printed with varying layer thickness, infill density, and patterns, then evaluated for tensile and morphological performance. The best tensile strength (39.13 MPa) occurred at 0.20 mm layer, 80% infill, and zigzag pattern, while poor bonding caused the lowest strength at 0.15 mm and 60% infill. Microstructural analysis confirmed uniform layers with minimal cracks, supporting their applicability in aerospace and biomedical sectors [1].

[*]Corresponding Author: senniangirinatarajan1987@gmail.com

The study examines how printing parameters affect the mechanical behaviour of Stone Fill Granite (50% stone powder) and Wood Fill (30% wood fibre) filaments compared to PLA. Tensile, compression, and bending tests showed that infill pattern, density, orientation, and shell count significantly alter stiffness and elasticity. Findings indicate consistent trends across PLA-based composites, supporting process optimization for biomechanical applications [2]. ZnO-reinforced PLA prototypes were evaluated for tensile, thermal, and shape-memory behaviour under different FDM settings. Peak strength values were achieved at 80% infill with tailored perimeter counts and patterns, while Young's modulus reached 233.68 MPa with honeycomb patterns [3]. Laser-tailored 3D printing enabled uniform dispersion of 16.1 wt. % TiC lamellae formed in situ from CNT-reacted Ti powder. The printed Ti-TiC composite achieved 912 MPa tensile strength and 16% elongation, representing a 350% improvement in combined performance over conventional Ti. Ultrafine grains and coherent TiC–Ti interfaces enhanced strength ductility synergy [4]. PLA compression strength was analyzed using FDM parameters layer thickness, infill density, and pattern by Taguchi L9 and ANOVA. Infill density dominated UCS variation (83.56%), whereas pattern and layer thickness had minimal effects [5]. Thirteen FDM parameters were studied for their influence on PLA mechanical properties including tensile, bending, warpage, and microhardness. Wall thickness, infill percentage, and layer thickness were major contributors depending on the property, with tensile strength heavily governed by wall thickness (31.83%) [6]. Tensile strength, hardness, and dimensional accuracy of the PLA were assessed under layer height, infill density, and print speed variations using Taguchi L9. Optimal tensile performance occurred at 70 mm/s, 0.2 mm layer, and 40% infill, while TGRA identified a unified optimum of 70 mm/s, 0.3 mm layer, and 40% infill. Confirmation tests validated improved overall performance [7]. PLA was modified with PEG and Ti particles to improve ductility, hydrophilicity, and cell compatibility in FDM-printed scaffolds. Combined PEG–Ti addition enhanced ductility without compromising strength and reduced contact angle by 25°. SEM confirmed improved roughness, adhesion, and biocompatibility compared to pure PLA [8]. This study set out to determine which of the proposed process factors would have the greatest impact on increasing the durability of 3-D printed components. This study's key factors were infill patterns (L, G, T and C), infill densities (40, 60, 80, 100%), layer thickness (120, 220, 320, and 420 μm), and nozzle temperatures (200º C, 215º C, 230º C, 245ºC) that varied. The originality of this research comes from its attempt to determine the best combination of these suggested parameters. In order to examine the material's strength, the research starts by making test samples utilizing a 25% TAP-PLA wire spool, following ASTM criteria. The next step is to examine the mechanical properties of the prototypes using, impact, tensile and flexural tests.

2 Materials and Methodology

Components were printed and its recycled equivalent, 25% TAP-PLA, underwent tensile, impact (Izod), and flexural testing in accordance with the relevant standards, namely ASTM D-638, ASTM D-790, and ASTM D-256. Table 1 shows the comprehensive list of the 3-D printer specification and FDM parameter properties. PLA is a good choice for 3-D printing and most common thermoplastics used at fused deposition modeling. The extensive use of polylactic acid filament in paper works, especially when discussing recycling of other filament types, was a deciding factor in its selection. In addition, PLA utilizes less energy in 3D printing because it is biodegradable thermoplastic polyester that comes from cleaner sources. The researchers in this study favored using Porima3D filament material for PLA filament because of its stellar reputation for quality. FDM-printed PLA samples were evaluated for surface finish quality using infill density, shell thickness, layer thickness, top/bottom layers, and infill overlap.

Optimal parameters improved micro-scale finish with minimal dimensional deviations [9]. For this work, the titanium alloy (TA) powder was sourced from Matrics Enterprises, Nagercoil, Tamilnadu, India. They are a certified supplier that focuses on high-purity metal and alloy powders for research and industrial purposes. The technical datasheet from the supplier specifies that the TA powder, in its as-received form with particle size distribution of 30 to 40 μm. The powder was first dried in an oven at 80°C for 12 hours to get rid of any moisture that remained, and then it was sieved through a 40-mesh stainless steel screen to make sure it was uniform and to get rid of any clumped particles.

Table 1. FDM parameters and its properties

Properties	Values
Printing speed (mm/min)	3000
Tolerance	± 0.1
Bed temperature (ºC)	60
Diameter of nozzle (mm)	0.4
Temperature of the nozzle (ºC)	200, 215, 230, 245
Layer thickness (μm)	120, 220, 320, 420
Infill density (%)	40, 60, 80, 100
Infill pattern	L, G, T and C
Filament type	25%FSP/PLA
Machine size (mm)	440×410×465
Diameter of filament (mm)	1.75
Printing method	FDM

The powder did not need any further chemical treatment because it was already pre-processed and metallurgically stable. Pellet extrusion and melt-mixing followed the usage of the uniformly dried TA powder. Mechanical testing was conducted on the resulting TA-reinforced filament in accordance with ASTM standards. An illustration of mechanical testing and extrusion process of a 25% TAP/PLA composite filament is depicted in Fig. 1. Standards according to ASTM D-638 were used to measure the samples' tensile strength [10]. The dimensions of these samples were as shown in Fig. 2: 33 mm for gauge length, 8 mm for gauge width, and 3 mm for thickness. We used a 5-ton capacity computerized universal testing equipment to determine the tensile strength. This apparatus for testing was outfitted with an environmental chamber that could precisely regulate temperatures within a range of -70ºC to 180ºC, with a margin of error of ±1ºC. Following the requirements laid out by ASTM D638 for the test, the sampling was carefully placed at an 82 mm grip distance. The experiment was conducted to find the tensile strengths of the samples at a cross-head speed of 2 mm/min. Fig. 3 shows the results of the flexural property evaluation according to the ASTM D790 criteria. We used the specified dimensions for the specimens, which were 90 mm long and 10 mm wide. Adjusting the flexural specimens' thickness to 3 mm brought them into compliance with the test machine's specifications. We used a specially-made flexural testing device with a 2 mm/min operational cross-head speed to perform the flexural three-point tests. The test specimens were prepared according to the ASTM D256 criteria for IS assessment. The particular measurements of these samples were as follows: 3 mm in thickness, 63 mm in length, 12.7 mm in width and a basic notch positioned at a 45-degree angle as shown in Fig. 4. Izod used an impact tester instrument with a 150 J rating to carry out the test. All of the samples were firmly fastened to the fixture in a vertical position with the sample's uneven edge facing the pendulum's conspicuous edge.

Afterwards, the pendulum could swing freely and hit the samples. To find the impact strength, the energy riveted before breakage was divided by the specimen's cross-sectional area (m^2), and the result was expressed as a kJ/m^2 ratio.

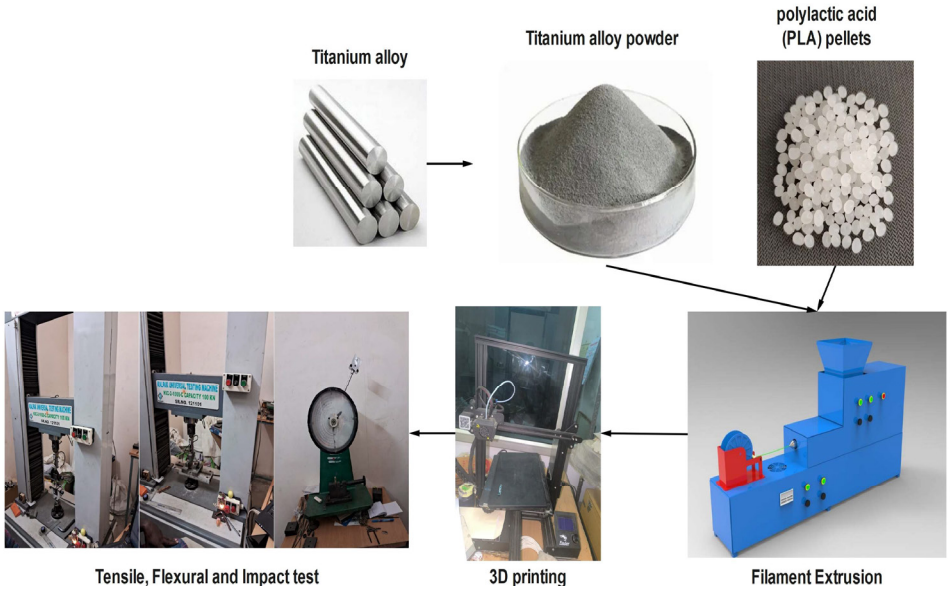

Fig. 1. An illustration of mechanical testing and extrusion process of a 25% TAP/PLA composite filament.

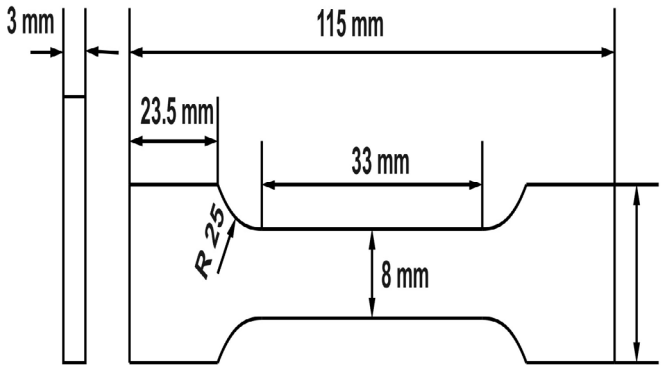

Fig. 2. Tensile test standards.

The Taguchi approach was used to find the best levels of the factors. After painstakingly designing the experiment with the L16 Taguchi orthogonal array, we were able to determine the appropriate factor levels by analyzing the results in detail. Table 2 lists the control parameters and the phases that correspond to Taguchi L16 experiment.

Table 2. Levels of input parameters

Notations	Parameters	Units	Level			
			1	2	3	4
A	Infill Pattern	–	(L)	(G)	(T)	(C)
B	Infill Density	%	40	60	80	100
C	Layer Thickness	µm	120	220	320	420
D	Nozzle Temperature	°C	200	215	230	245

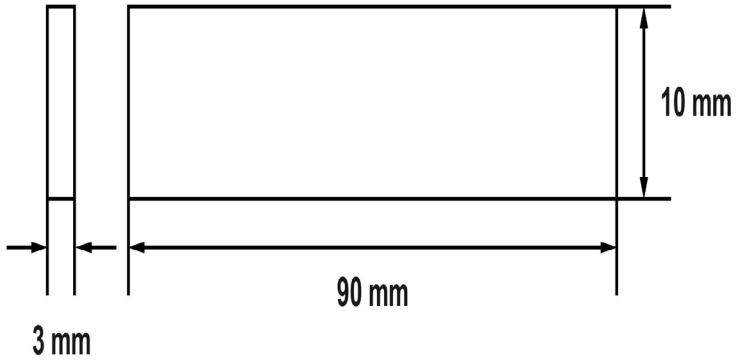

Fig. 3. Flexural test standards.

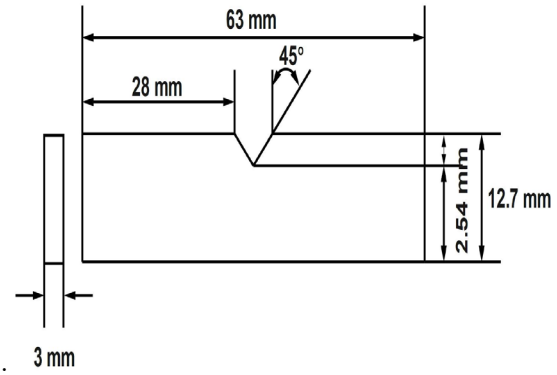

Fig. 4. Impact test standards.

3 Results and Discussion

Fused deposition modeling printer were used to create three specimens for every experimental session. Table 3 displays mean values from three specimens for UTS FS (flexural strength), IS (impact strength), and (ultimate tensile strength), providing representative outcomes. As an evaluation metric for eminence characteristics, the Taguchi technique sets up test parameters by translating objective values as signal-to-noise ratios. Control elements are those that the designer has decided upon, whereas noise aspects include things like temperature and humidity. By utilizing the signal-to-noise ratio, the Taguchi approach builds a resilient system that is less affected by noise. Factor weighting, lowering crosstalk, improving overall superiority, optimizing quality design with little variation, and addressing processing means and variability all benefit greatly from leveraging the S/N ratio. The objective of this work is to enhance the mechanical efficiency of 25%TAP-PLA components adjusting parameters like nozzle temperature, infill pattern, infill density, and layer thickness. In optimization, the "larger the better" principle serves as a compass. PLA reinforced with milled carbon fibre was optimized using Taguchi L16 and ANOVA to determine tensile behaviour [11]. Table 4 displays the results of the Taguchi L16 orthogonal array test along with the signal-to-noise ratio (S/N), which are the exact values of the strengths.

Table 3. Taguchi L16 Orthogonal array

S. No.	A	B (%)	C (µm)	D (°C)	TS (MPa)	FS (MPa)	IS (kJ/m^2)
1	L	40	120	200	49.64	79.39	13.66
2	L	60	220	215	51.54	93.14	14.62
3	L	80	320	230	54.91	97.79	16.03
4	L	100	420	245	53.5	89.02	14.93
5	G	40	220	230	51.79	91.69	16.96
6	G	60	120	245	54.36	82.44	16.4
7	G	80	420	200	53.64	98.71	17.71
8	G	100	320	215	56.31	94.68	17.37
9	T	40	320	245	52.2	79.22	15.32
10	T	60	420	230	52.72	80.59	15.73
11	T	80	120	215	54.71	95.85	16.35
12	T	100	220	200	53.96	93.79	17.12
13	C	40	420	215	51.51	84.44	15.53
14	C	60	320	200	50.99	81.15	15.89
15	C	80	220	245	53.19	95.33	16.95
16	C	100	120	230	53.29	90.55	18.13

Table 4. Findings from S/N ratios and the Taguchi L16 orthogonal array test

S. No.	TS (MPa)		FS (MPa)		IS (kJ/m^2)	
	Means	S/N Ratios	Means	S/N Ratios	Means	S/N Ratios
1	49.64	33.92	79.39	38.00	13.66	22.71
2	51.54	34.24	93.14	39.38	14.62	23.30
3	54.91	34.79	97.79	39.81	16.03	24.10
4	53.5	34.57	89.02	38.99	14.93	23.48
5	51.79	34.28	91.69	39.25	16.96	24.59
6	54.36	34.71	82.44	38.32	16.4	24.30
7	53.64	34.59	98.71	39.89	17.71	24.96
8	56.31	35.01	94.68	39.53	17.37	24.80
9	52.2	34.35	79.22	37.98	15.32	23.71
10	52.72	34.44	80.59	38.13	15.73	23.93
11	54.71	34.76	95.85	39.63	16.35	24.27
12	53.96	34.64	93.79	39.44	17.12	24.67
13	51.51	34.24	84.44	38.53	15.53	23.82
14	50.99	34.15	81.15	38.19	15.89	24.02
15	53.19	34.52	95.33	39.58	16.95	24.58
16	53.29	34.53	90.55	39.14	18.13	25.17

3.1 Impact of Process Parameters on Tensile Behavior

All samples that were 3D printed had their tensile strengths measured using a UTM. Below is a summary of the 25% TAP-PLA material's UTS across several experimental conditions, as shown in Table 5. A regression equation and process parameter optimization were both based on these findings. TS raised with increasing specific infill patterns and infill densities, dropped with higher nozzle temperatures and layer thicknesses and showed significant trends in the main effects plot. Fig. 3 shows the main effect plot, that describe the stages and consequences of the parameters in an easy way. Among the test parameters, the infill density is by far the most important. Increases in both the thickness of the layers and the temperature within the nozzle reduced the tensile strength by weakening the interfacial bonding that prevented the formation of cavity.

Different infill patterns affected interlayer diffusion, and increasing the material infill percentage strengthened the portion. The TS of the tested shapes were highest for grid design, then for the line, concentric, and triangular patterns. The extra contact points made possible by the wavy grid infill design were especially important in achieving this improved strength.

Table 5. Response table for S/N ratios (tensile strength)

Level	A	B (%)	C (µm)	D (°C)
1	34.38	34.20	34.48	34.32
2	34.65	34.38	34.42	34.56
3	34.55	34.67	34.58	34.51
4	34.36	34.69	34.46	34.54
Delta	0.29	0.49	0.16	0.24
Rank	2	1	4	3

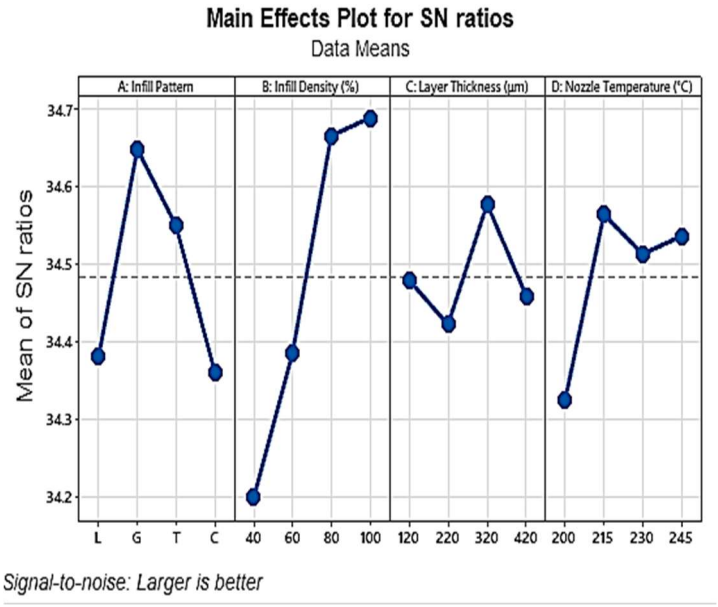

Fig. 5. Tensile strength S/N ratios.

Fig. 5 shows the tensile strength S/N ratios. As a result, the grid infill pattern works great for making strong things with less material. Following optimization, the optimal setup included a 100% infill volume, a nozzle temperature of 215ºC a layer thickness of 320 µm and grid printing pattern resulting in extreme TS of 56.31 MPa. In another study, Cu-PLA parts printed by FDM were studied and results showed higher layer thickness and infill increase both part weight and maximum failure load, peaking at 230 N with a 0.5 mm layer and Tri-Hexagonal pattern. Multi-objective optimization identified 0.152 mm layer thickness, 32.9% infill, and Grid pattern as optimal [12]. Table 6 displays the results of an ANOVA for the obtained experimental data, which additionally investigated the relevance of each process parameter. Fig. 6 shows the tensile strength that was acquired from our modeling efforts as an average probability graph. To evaluate the precision of the model, this graph is an excellent resource. The normality graph shows that residues follows normal distribution, since all of the P-values are greater than 0.05 threshold. As a result, it is clear that our research fits well with the theoretical framework.

In addition, our experimental model is balanced and accurate since the distribution is close to the center axis. In another study, copper-filled PLA (65% Cu) specimens were studied for tensile strength under variations in temperature, flow rate, and layer thickness. Temperature and flow rate were dominant contributors, accounting for 42.41% and 22.16% of strength variation. Optimization identified 220°C temperature, 110% flow rate, and 0.189 mm layer thickness for maximum strength [13].

Table 6. ANOVA for tensile behaviour

Source	DF	Seq SS	Contribution	Adj MS	F-Value	P-Value
A	3	8.562	19.94 %	2.8541	3.33	0.175
B (%)	3	24.540	57.15 %	8.1801	9.53	0.048
C (μm)	3	2.125	4.95 %	0.7082	0.83	0.561
D (°C)	3	5.137	11.96 %	1.7123	2.00	0.292
Error	3	2.575	6.00 %	0.8583		
Total	15	42.939	100.00 %			

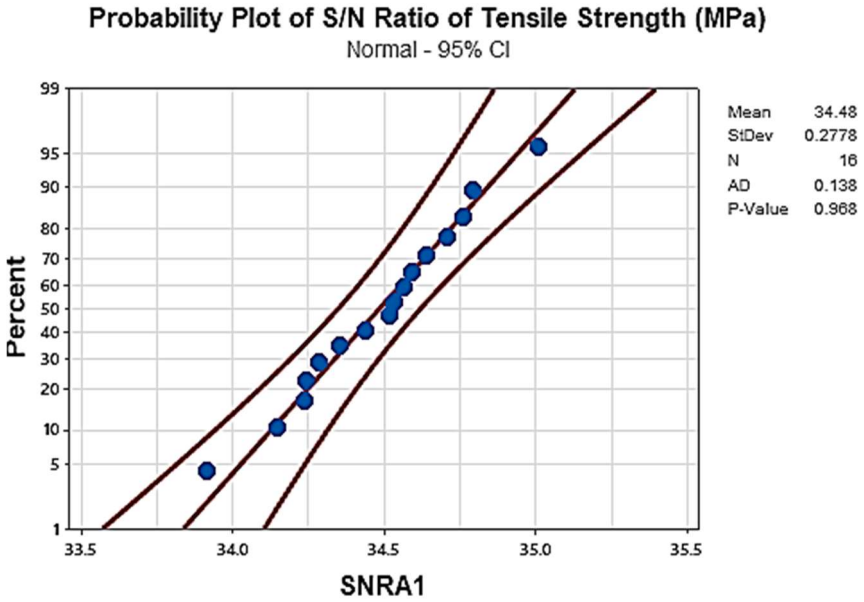

Fig. 6. Tensile strength probability plot.

3.2 Impact of Parameters on Flexural Strength

When looking at P-value from analysis of variance results, we can see that the highest flexural strength for the PLA that was 25 % reinforced with titanium alloy powder was 98.71 MPa.

Table 7. Variance analysis

Source	DF	Seq SS	Contribution	Adj MS	F-Value	P-Value
A	3	50.93	7.04 %	16.976	2.79	0.211
B (%)	3	486.49	67.21 %	162.162	26.62	0.012
C (μm)	3	99.87	13.80 %	33.291	5.46	0.098
D (°C)	3	68.25	9.43 %	22.749	3.73	0.154
Error	3	18.28	2.53 %	6.092		
Total	15	723.81	100.00 %			

Fig. 7 shows that the most important factors that contributed to the maximum values of flexural properties were a nozzle temperature of 215°C, a layer thickness of 220 µm, an infill density of 80% and an infill pattern of a grid, as shown in the mean plot, which helped to find the best parameters for FS utilization. In addition, the results of an ANOVA provide ideas on how various process parameters can affect the final product. There was clearly no influence on the flexural qualities from layer thickness, nozzle temperature or infill pattern since none of these factors significantly affected flexural strength. When contrasted with other factors such as layer thickness, nozzle temperature and infill pattern, infill density stood out as the most significant one. Infill plays a crucial role as a support bridge between flooring layers and upper ceiling. The reinforcement's load-bearing capacity drops and its flexural characteristics get worse and infill pattern gets less dense.

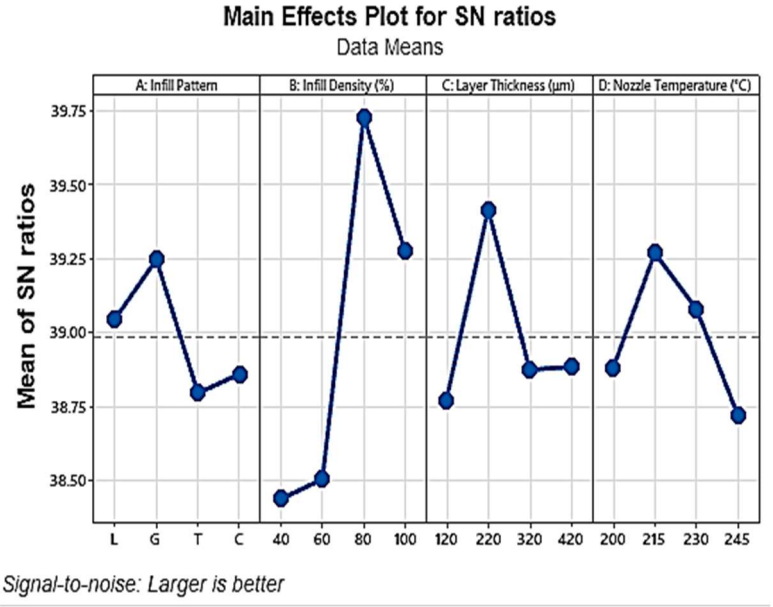

Fig. 7. For flexural strength, S/N ratios.

The results from table 7 shows the interaction values of the task obtained. Fig. 6 shows the normal probability plot of the flexural strength data. The goal of this visual representation is to ensure that the model is accurate. The normality graph indicates that residuals adhere normal distribution because all of the P-values are greater than 0.05 criterion. It is clear that our research fits well with the theoretical framework. In addition, the closeness to central axis shows how accurate and persistent the recognized model is. It is clear that the model is accurate because of the balanced distribution. Plot of probability for flexural strength is shown in Fig. 8. Table 8 shows the S/N ratio response table for flexural strength.

Table 8. S/N ratio response table (flexural strength)

Level	A	B (%)	C (µm)	D (°C)
1	39.04	38.44	38.77	38.88
2	39.25	38.50	39.41	39.27
3	38.79	39.73	38.87	39.08
4	38.86	39.27	38.88	38.72
Delta	0.45	1.29	0.64	0.55
Rank	4	1	2	3

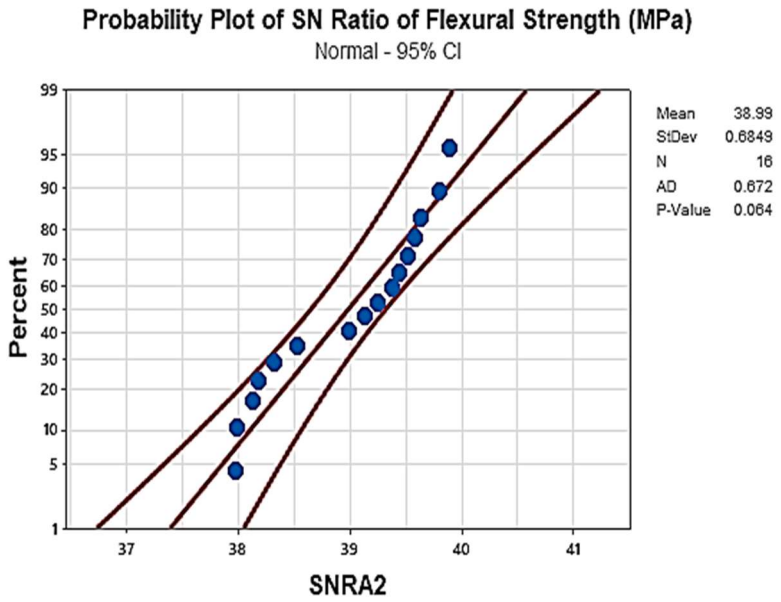

Fig. 8. Plot of probability for flexural strength.

3.3 Effect of Process Parameter on Impact Behavior

Table 9 shows that the 3D-printed composite had an impact strength of 18.13 kJ/m^2 at its maximum. Based on P-value from analysis of variance results in Table 9, it is clear that there is a statistically significant relationship between infill pattern, layer thickness, infill density and nozzle temperature. A nozzle temperature of 230ºC, a 220 µm layer thickness, 100% infill density, and a grid infill pattern were the parameters that led to this high performance.

Table 9. Variance analysis

Source	DF	Seq SS	Contribution	Adj MS	F-Value	P-Value
A	3	11.7673	54.64 %	3.9224	18.01	0.020
B (%)	3	7.0680	32.82 %	2.3560	10.82	0.041
C (µm)	3	0.3934	1.83 %	0.1311	0.60	0.656
D (°C)	3	1.6553	7.69 %	0.5518	2.53	0.233
Error	3	0.6533	3.03 %	0.2178		
Total	15	21.5374	100.00 %			

Fig. 9 shows the (S/N) percentage for different impact strengths, which provides more information. Table 10 shows the results for signal-to-noise ratios, where higher values are an improvement. In terms of importance, the infill pattern trumped all of the other factors including layer thickness, nozzle temperature and infill density among those characteristics.

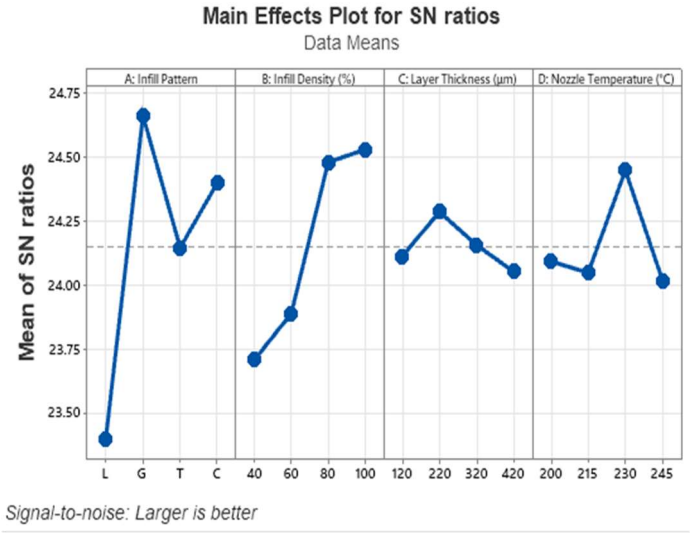

Fig. 9. S/N ratios for the impact force.

Table 10. S/N ratio response table (impact strength)

Level	A	B (%)	C (µm)	D (°C)
1	23.40	23.71	24.11	24.09
2	24.66	23.89	24.29	24.05
3	24.15	24.48	24.16	24.45
4	24.40	24.53	24.05	24.02
Delta	1.26	0.82	0.23	0.43
Rank	1	2	4	3

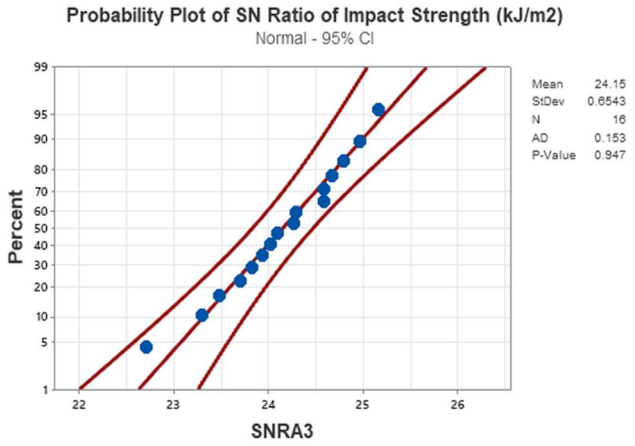

Fig. 10. Strength of impact probability plot.

Fig. 10, shows normal probability curve for impact strength, were very important for evaluating accuracy of model. Importantly, all of P-values in normalcy graph were more than the 0.05 level, which means that the residues really follow normal distribution. This means that mathematical model and experimental study were perfectly congruent with each other. The closeness of distribution to the central axis were another indicator of accuracy and reliability of model. component, outperforming nozzle, layer thickness, and infill density.

Fig. 10 shows that when the infill pattern and impact resistance increase, the density value also increases.

3.4 SEM Evaluation

Fig. 11 shows scanning electron micrographs of fractured test parts from the impact, flexural, and tensile protocols. The images were taken by Zeiss Gemini model at fracture angle particularly at the fracture locations, and in regions with plastic deformation. During testing, the machine captures micrographs of the fracture surfaces between a voltage range of 200 V to 30 kV. Air bubbles form between the layers, resulting in less-than-ideal bonding.

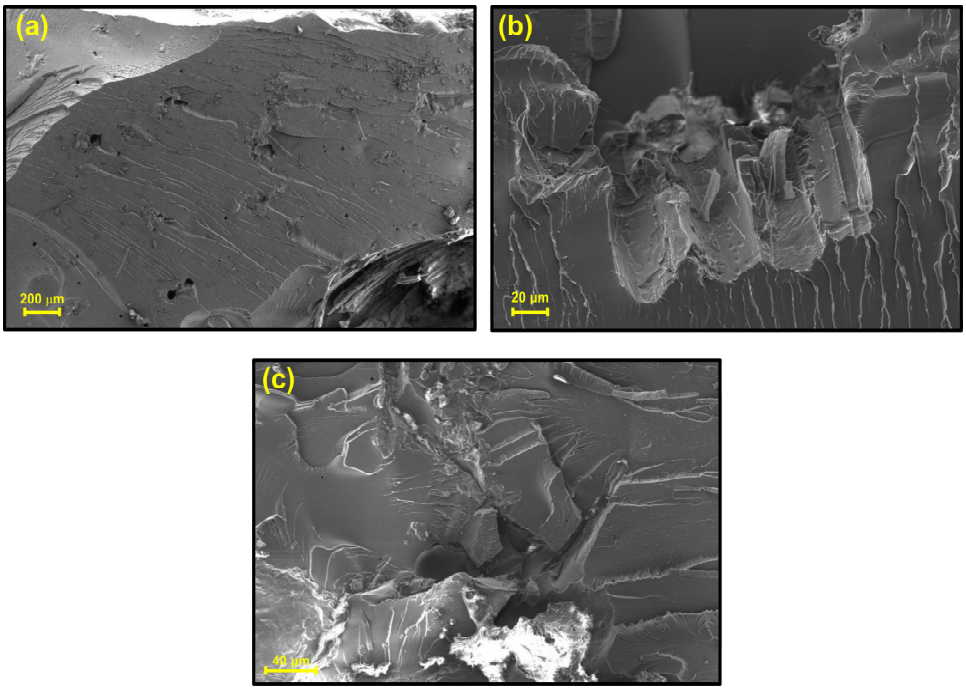

Fig. 11. SEM examination of broken surfaces at ideal test components for impact, flexural, and tensile strength.

These holes interrupt the flow of heat during production, which is what causes the long-term strains. Tensile, flexural, and impact behavioral performance were all negatively impacted by these gaps. Fractography revealed pores, delamination, and weak bonding as key failure features [14]. The trial components are also less resistant to distortion because of their absorbent structure and surface pores. Similar layers created using the fused deposition modeling (FDM) technique are clearly visible in cross-sectional view of broken experimental components. Large voids and surface porosity allow test deformation, as shown in Fig. 11 (b), which illustrates gaps between the components. As a result of filament melting and opening of pores at PLA 3D printing, the mechanical strength of the test item has been slightly reduced. The manufacturing procedure does reduce the strength of the PLA filament, but it still performs better than 25% titanium alloy powder-reinforced PLA (25% TAP-PLA). In the scanning electron micrographs, the polylactic acid material shows signs of surface roughness due to its brittle fracture characteristic. This roughness is a result of fracture-related localized pressures.

Our study's main conclusion is that mechanical properties are most strongly affected by layer thickness. Increasing the thickness of a polylactic acid layer usually enhances the material's mechanical characteristics. The low melting point and user-friendliness of PLA make it a popular material. Polylactic acid compounds, whether virgin or recycled, show strikingly similar spectrum characteristics. With mean-based estimation working better than Taguchi's logarithmic conversions, the results generated from Taguchi analysis [15]. Table 11 shows the comparison between experimental validation and optimized setup correspondingly.

Table 11. Comparison between experimental validation and optimized setup

	A	B (%)	C (µm)	D (°C)	TS (MPa)	FS (MPa)	IS (kJ/m^2)
8th Run	Grid	100	320	215	56.31	94.68	17.37
Experiment	Grid	80	220	230	51.79	91.69	16.96
Predicted	Grid	80	220	230	18.23	99.47	55.87

4 Conclusion

Finally, this research used fused deposition modeling to examine the mechanical characteristics of PLA filaments reinforced with 25% titanium alloy powder. We systematically experimented with different production settings to observe how they affected mechanical performance. The findings are given below: The most important characteristic that improved mechanical properties was infill density. Scanning electron microscopy revealed that surface holes and cracks enabled deformation. Remaining tensions, caused by air gaps seen in SEM images, had a negative impact on mechanical characteristics. The production process reduced the material's strength slightly, yet the regression model still accurately predicted the mechanical properties. We were able to determine the best parameters for the filament material (25% TAP-PLA), nozzle temperature (230ºC), layer thickness (320 µm), infill pattern (grid) and infill density (100%). The computed strengths encompass TS of 51.79 MPa, FS of 91.69 MPa, and IS of 16.96 kJ/m^2.These numerical findings provide information on how to enhance the mechanical efficiency of printed parts by fine-tuning 3D printing procedures using 25% TAP-PLA filaments.

References

1. A. Shrivastava, J. S. Chohan, R. Kumar, On mechanical, morphological, and fracture properties of sustainable composite structure prepared by materials extrusion-based 3D printing. Journal of Materials Engineering and Performance. **33**, 8778 (2024). https://doi.org/10.1007/s11665-023-08593-y
2. M. Mencarelli, L. Puggelli, Y. Volpe, B. Innocenti, Sensitivity on 3D-printed parameters of stiffness and Young's modulus of FDM-printed PLA, StoneFilTM granite and Wood Fill filaments: a comparative analysis. Journal of Mechanics in Medicine and Biology. **7**, 572 (2025). https://doi.org/10.1142/S0219519425400548
3. V. P. Suresh Kumar, S. Seenivasan, G. B. Loganathan, P. Jayanthi, R. Girimurugan, S. Hasane Ahammad, Enhancing Mechanical Properties of PLA/Kevlar Fiber Composites with ZrO_2 Nanorod Interface Modification for High-Performance Applications. Advances in Science, Technology & Innovation (2024). https://doi.org/10.1007/978-3-031-63909-8_28
4. M. Al-Wswasi, W. A. Al-Khaleeli, S. A. Aufy, Implement the artificial neural network concept for predicting the mechanical properties of printed polylactic acid parts. Archives of Metallurgy and Materials. **19**, 73 (2025). https://doi.org/10.12913/22998624/201463

5. M. Sengottaiyan, S. Eswaran, R. Amal Quais, S. Rokumar, S. Rohan, Enhancing Compressive Strength of Additively Manufactured Polylactic Acid Composites using Simultaneous Impregnation Extrusion and Carbon Fiber Reinforcement. Malaysian Journal of Chemistry. **27,** 427 (2025). https://doi.org/10.55373/mjchem.v27i3.427
6. A. S. Khusheef, R. Hashemi, M. Shahbazi, Optimizing FDM process parameters: predictive insights through Taguchi, regression, and neural networks. Physica Scripta. **99**, 065201 (2024). https://doi.org/10.1088/1402-4896/ad42d7
7. K. Patel, S. Acharya, G. D. Acharya, Multi objective optimization of FDM parameters using Taguchi grey relation analysis for PLA specimen. Jurnal Kejuruteraan. **36**, 113 (2024). https://doi.org/10.17576/jkukm-2024-36(1)-11
8. R. Girimurugan, M. Vairavel, A.A. Moorthy, E. Prakash, S. Madheswaran, Experimental Studies on Mechanical Behaviour of Polylactide (PLA) Matrix-Aluminium Oxide (Al_2O_3) Particles Reinforced Composites. Advances in Materials Research. 589 (2019). https://doi.org/10.1007/978-981-15-8319-3_58
9. M. Sengottaiyan, S. Eswaran, M. Sathish, S. Sudharsan, A. Thanish Samson, Influence of Printing Parameters on the Strength and Toughness of 3D-Printed Composites. In EPJ Web of Conferences. **336,** 02003 (2025). https://doi.org/10.1051/epjconf/202533602003
10. P. Anerao, A. Kulkarni, Y. Munde, N. Wasatkar, A comparative study of machine learning techniques for predicting mechanical properties of fused deposition modelling (FDM)-based 3D-printed wood/PLA biocomposite. Mechanics & Advanced Composite Structures. **12**, 261 (2025). https://doi.org/10.22075/macs.2024.33776.1638
11. V. Mishra, N. Bharat, V. Kumar, M. Vellaisamy, D. Veeman, Multi-objective optimization of 3D printed PLA/carbon fibre composite using a combined approach of gray relational analysis and ANOVA. Journal of Reinforced Plastics and Composites. **38**, 4208 (2025). https://doi.org/10.1177/08927057251339246
12. P. Thangavel, S. Vignesh, R. Sureshkumar, A. Gowrishankar, R. Girimurugan, Study on mechanical properties of polylactic acid matrix added with fly ash and tamarind kernel powder micro fillers. NanoWorld J. **9(S1),** S626 (2023).
13. M. Moradi, O. Mehrabi, F. A. Rasoul, A. A. Mattie, F. Schaber, R. Khandan, Enhancing 3D printing copper-PLA composite fabrication via fused deposition modeling through statistical process parameter study. Micromachines. **15**, 1082 (2024). https://doi.org/10.3390/mi15091082
14. K. R. Kumar, M. Gokul, M. Kumar, Investigations on mechanical properties and characterisation of polylactic acid/aluminium metal infill polymer composites manufactured by fused deposition modelling. Journal of Materials Engineering and Performance. **33**, 8857 (2024). https://doi.org/10.1007/s11665-023-08572-3
15. M. Easwaramoorthi, A. Giridharan, K. Nandhakumar, E. Pradeep, G. Rangith, Mechanical Characterization and Predictive Analysis of Flax Fiber/PLA Honeycomb Sandwich Structures in FDM Additive Manufacturing. In E3S Web of Conferences. **559,** 02010 (2024). https://doi.org/10.1051/e3sconf/202455902010